Measuring the Neutron Lifetime with Magnetically Trapped Ultracold Neutrons

H. P. MUMM*, M. G. HUBER. A. T. YUE†, A. K. THOMPSON. M. S. DEWEY

National Institute of Standards and Technology,
Gaithersburg, MD 20899, USA
**E-mail: hans.mumm@nist.gov*
†Previous affiliation: Institute for Research in Electronics and Applied Physics,
University of Maryland, College Park, MD 20742

C. R. HUFFER, P. R. HUFFMAN, K. W. SCHELHAMMER

Physics Department, North Carolina State University,
Raleigh, NC 27699, USA

C. O'SHAUGHNESSY

University of North Carolina, Chapel Hill, NC 27599

K. J. COAKLEY

National Institute of Standards and Technology,
Boulder, CO 80309, USA

We describe an experiment to measure the neutron lifetime using a technique with a set of systematic uncertainties largely different than those of previous measurements.[1] In this approach, ultracold neutrons (UCN) are produced by inelastic scattering of cold (0.89 nm) neutrons in a reservoir of superfluid ^{4}He.[2] These neutrons are then confined using a three-dimensional magnetic trap. As the trapped neutrons beta decay, the energetic electrons produced in the decay generate scintillations in the liquid He;[3,4] each decay is detectable with nearly 100 % efficiency. The neutron lifetime can be directly determined by measuring the scintillation rate as a function of time.

Keywords: Neutron Lifetime; Magnetic Trapping

1. Introduction

Our method for measuring the neutron lifetime utilizes ultracold neutrons (UCN) confined within a three-dimensional magnetic trap. As the interaction between the neutron's magnetic moment and the trap magnetic field $\vec{B}$

conserves energy, neutrons must dissipate energy within the trapping region by other means. This occurs when 12 K neutrons (0.89 nm) downscatter in superfluid ^{4}He to near rest via single phonon emission.[2] When the neutron's spin is parallel to the magnetic field (low-field-seeking state), it will seek to minimize its potential energy by moving toward low field regions. The trap is designed such that field gradients are sufficiently small that the neutron's spin direction adiabatically follows the direction of the magnetic field. Thus, UCN with energies below the potential difference between the center and edge of the trap (trap depth) and in the low-field-seeking state (half of those downscattering from the unpolarized beam) will be trapped by the magnetic field. UCN with the opposite spin state can experience some material confinement from the material wall of the trap, but are quickly lost through upscattering.

The UCN population is thermally detached from the helium bath allowing accumulation of UCN to a density as high as $P\tau$, where P is the superthermal production rate and τ is the UCN lifetime in the trap. Neutron decay events are detected by turning off the cold neutron beam and observing the scintillation light created by the beta-decay electrons (endpoint energy of 782 keV). When an electron moves through liquid helium, it ionizes helium atoms along its track. These helium ions quickly recombine into metastable He_2^* molecules. About 24 % of the initial electron energy goes into the production of extreme ultraviolet (EUV) photons from singlet decays, corresponding to approximately 15 photons/keV.[6] These EUV photons are frequency down-converted to blue photons using the organic fluor tetraphenyl butadiene (TPB) coated onto a diffuse reflector (Gore-Tex) surrounding the trapping region. This light is transported via a series of optical elements to room temperature and detected by two photomultiplier tube (PMT)s operating in coincidence. Our detection method allows the observation of neutron decay events *in situ*, and therefore to directly measure the decay curve.

2. Apparatus

At the heart of our apparatus is a high-current Ioffe-type magnetic trap.This trap consists of an accelerator-type superconducting quadrupole magnet that provides radial confinement, combined with two aligned low-current solenoids that provide axial confinement. The quadrupole magnet, which operates at a current of up to 3,400 A, is on loan from the High Energy Accelerator Research Organization (KEK) laboratory in Japan. The two solenoids, which operate up to 250 A, were designed and constructed in

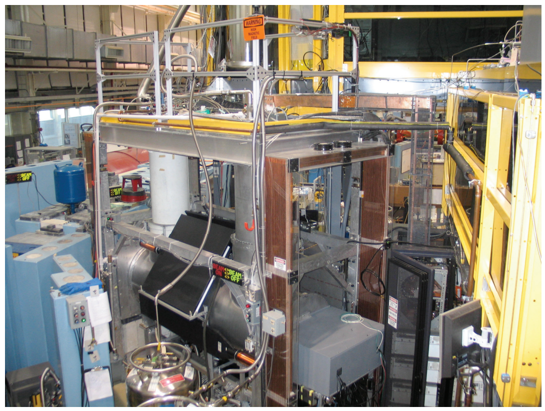

Fig. 1. The neutron lifetime apparatus on the NCNR beamline.

collaboration with American Magnetics, Inc.[7] The trap has a trapping volume of 8 l and can be operated at a depth of up to 3.1 T, although in practice a variety of depths were used for systematic and stability reasons.

A pair of 5,000 A High-Temperature Superconducting (HTS) current leads[8] on loan from FermiLab are used to bring the current from the room-temperature power supplies into the liquid helium. We designed and built a second set of HTS leads in-house for the 250 A solenoids. These two sets of leads reduce the heat input to the helium bath from a total of 8.8 W to 0.9 W as compared to conventional leads. Finally, to further reduce helium consumption and lower lead operating temperature, we incorporated a two-stage cryocooler with 1.5 W of cooling power at 4.2 K into the apparatus. This trap assembly was operated in a custom cryostat (Fig. 1) and reached > 85 % of full current before the first quench. However, due to the need to ramp the magnets on short timescales relative to the neutron lifetime, and the subsequent magnet instabilities this introduced, most data was taken at approximately 70% of design depth.

On the beam-entrance end (Fig. 1, left side), a vertical tower houses an Oxford 400 dilution refrigerator used for cooling the helium-filled cell. The second tower near the light collection system (Fig. 1, right side) houses the current leads for the trap, supplies liquid helium for the magnet and contains the thermometry, cryogen monitoring, and magnet voltage taps.

Cold (0.89 nm) neutrons enter the trapping region through a series of Teflon (vacuum) and beryllium (thermal) windows on the dewar.[9–11] Interlocking tubes of boron nitride (BN) surround the beam and shield the dewar from scattered neutrons to minimize backgrounds from neutron-induced activation. Near the front window of the helium cell the BN is coated with graphite to reduce light scattering. Neutrons scattered out of the beam are absorbed by high-purity BN shielding exterior to the light detection system while the remaining beam is absorbed at the end of the cell by the acrylic light guide. Neutrons absorbed in the acrylic do not cause significant color center formation at our present beam intensity and hence do not degrade the light detection efficiency. Thin carbon tubes line the inside of the BN to absorb any neutron-induced luminescence from color center formation in the BN. The nearly isotopically pure ^{4}He, acrylic light guides, and shielding assembly are housed in a stainless steel tube that extends through the length of the magnet. This cell is cooled to $T <$ 300 mK to reduce phonon upscattering. To minimize eddy-current heating, the refrigerator is thermally connected to the trapping region (cell) using a superfluid helium heat link as opposed to copper links. The 26 kg cell is thermally isolated using 6 Zylon support fibers.

In principle, trapped neutrons travel in the helium undisturbed until they beta-decay. Each decay is detectable with very high efficiency (depending on cuts). The light detection system is shown in Fig. 2 and consists of a 9 cm outer diameter Goretex tube with a thin layer of TPB evaporated onto the inner surface. The end of the tube is viewed by a 9 cm diameter acrylic rod that transports the light outside the magnet bore. The light exits the low temperature region through a 5 mm thick acrylic window at the end of the trapping cell, passes through both a 6 mm thick acrylic window and a 1.5 mm quartz window at 4 K, and then into a 11.4 cm diameter acrylic rod that transports the light outside of the apparatus. Once exiting the vacuum region, light is collected via a non-imaging Winston cone and divided using a Y-shaped acrylic splitter to couple the light into two 12.7 cm diameter PMTs that are operated in coincidence mode to reduce uncorrelated low-temperature luminescence, dark-current noise and helium after-pulsing.

Pulses are digitized using transient waveform digitizers and stored for off-line analysis. This allows one to vary discrimination thresholds as well as perform pulse-shape discrimination (PSD). Background events arising from cosmic rays passing through either the acrylic or helium are tagged with approximately 30% efficiency using an array of scintillation paddles. Radiation from instruments in the surrounding area also introduce background events. The apparatus is shielded on the neutron entrance and reactor (south) sides by walls consisting of 10 cm of lead, 5 cm of polyethylene,

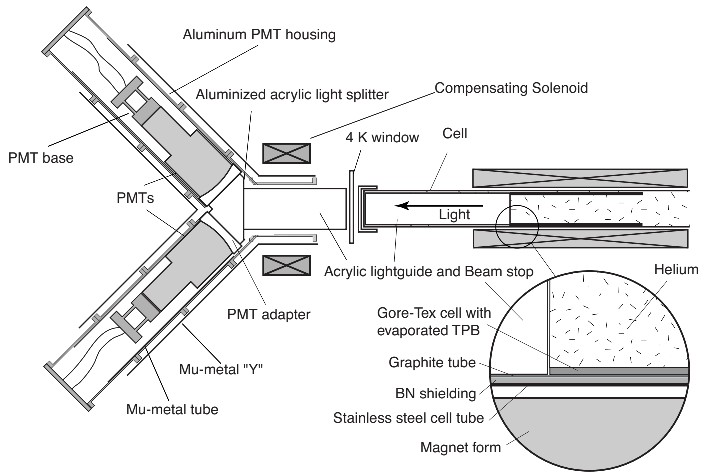

Fig. 2. Light collection system.

and Boroflex sheets and concrete blocks on the north side . The remaining backgrounds arise from neutron-induced activation of materials within the detection region, neutron-induced luminescence, and gamma-rays Compton scattering within the acrylic.

3. Systematic Effects

In the following discussion we provide an overview of our three largest potential systematic effects and our knowledge of each. However, we emphasize that continued studies of systematic effects are underway and in most cases we describe ongoing work.

3.1. *Marginally Trapped Neutrons*

Neutron loss during the measurement process, resulting in a systematic shift in the measured lifetime, is a reoccurring problem in UCN experiments. In our apparatus, UCN with energies both above and below the trap threshold are produced during the trap loading stage. The vast majority of *above-threshold* neutrons are absorbed or up-scattered by the materials of the trap wall before data collection begins, and therefore do not affect the measurement. A small fraction, however, remain in the trap for finite times before β-decaying due to a combination of two mechanisms: marginally trapped quasi-stable orbits and material bottling. Here we present a brief description of our work to understand these effects, more detailed discussions can be found elsewhere.[10,11]

In support of earlier versions of the apparatus we developed a simplified 3-D analytical model for neutron loss. With this simple model, we were able to show that briefly ramping the trap to a lower field could remove a fraction of above threshold neutrons from the trap. Significantly, this analysis suggested that with a higher-field magnet, field ramping should result in considerably more efficient purging of above threshold neutrons than in shallower traps.

The development of a complete numerical simulation of neutron trajectories and wall interactions is now underway, however it is complicated by the occurrence of chaotic scattering. Although the trajectories of above-threshold neutron with escape times longer than 5 - 10 s in general can not be precisely tracked, we assume the mean survival time of an ensemble of neutrons is well determined at any time of interest.[12] Thus, simulation allows us to study the coupling between and axial and radial components of the trajectory, and estimate the time-dependent survival probability of above threshold UCN.

The previous trap, due to its shallow depth, exhibited strong material bottling. For the new KEK trap however, because the above-threshold neutrons gain more kinetic energy during a ramp, they have a higher probability to penetrate the wall potential, reducing this effect. From simulations, we can then find the ramping conditions under which we can purge practically all UCN and achieve a negligible systematic error.[10]

As a way of benchmarking these simulations we have focused on determining the systematic error in the lifetime estimate due to above threshold UCN for the KEK trap at 70 % maximum strength for two bounding material wall potentials in cases where the magnetic field is static (i.e. the field is not ramped). In one case, the cylindrical surface wall loss probability is predicted according to the multilayer potential associated with the various wall materials, Fig. 3.[13] In the second case, an upper bound on incoherent scattering is added. Although these models predict very different wall loss probabilities, the systematic errors associated with the two models are similar, $\Delta_\tau = -30.1 \pm 3.3$ s and $\Delta_\tau = -30.0 \pm 2.7$ s. We note that this is the estimated shift in the trap lifetime with no field ramping. Initial simulations that take into account ramping the quadrupole field from the initial 70 % field strength to 50 % reduce this systematic effect to less than 3 s. In future measurements, we anticipate ramping to lower field values will further ameliorate the effect.

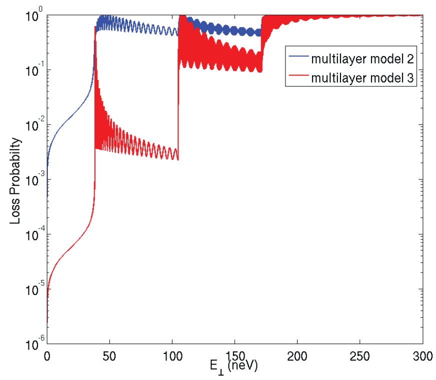

Fig. 3. The multi-layer models for the material wall potential used in modelling above-threshold neutrons.

Through a combination of analytic and numerical models, we are developing an understanding of systematics related to above threshold neutrons systematic and are refining our understanding of the conditions under which the probability of retaining significant of these neutrons is negligible. In addition, this systematic can also be experimentally tested by taking lifetime data at different minimum values of the field ramp. With the higher counting statistics afforded by the KEK magnet, one can experimentally quantify the field ramping technique and these measurements as benchmarks to further refined Monte Carlo models.

3.2. ^{3}*He Purity*

The isotopic ratio of natural helium $R_{34} = ^3\text{He}/^4\text{He}$ is 1.3×10^{-6} for atmospheric helium and $(1-2) \times 10^{-7}$ for commercial helium extracted from natural gas wells.[14] For the lifetime experiment, it is essential to have significantly increased isotopic purity; the UCN loss rate Γ_{abs} due to absorption by ^{3}He is $\Gamma_{abs} = nR_{34}\sigma_{th}v_{th}$, where $n = 2.17 \times 10^{22}$ cm^{-3} is the number density of helium atoms, $\sigma_{th} = 5330$ b is the thermal neutron capture cross section, and $v_{th} = 2200$ m/s is the thermal neutron velocity. Thus a purity of $R_{34} < 10^{-15}$ is required to reduce the correction from the ^{3}He absorption to $< 2 \times 10^{-5}\tau_n$.

This purity has been demonstrated previously in 1978 by McClintock *et al.*[15] where, using helium produced using the heat flush technique from the same apparatus that produced our helium, an isotopic purity of $< 10^{-15}$ was indirectly measured using Accelerator Mass Spectroscopy (AMS) after reverse concentration. However, in order to demonstrate the required purity with a direct measurement, we have been collaborating with the AMS group at the Argonne Tandem Linac Accelerator System (ATLAS) facility at Argonne National Laboratory (ANL). We believe that the results from our latest series of runs show that the facility will be capable of making AMS measurements with sufficient sensitivity for our needs; isotopic ratio measurements with AMS can typically reach a maximum sensitivity of $10^{-15} - 10^{-16}$.

The advantage of AMS is that by accelerating ^{3}He to approximately MeV energies and passing them first through a stripper foil and then into the split pole spectrometer at ATLAS, the $^3He^{2+}$ ion peak can be unambiguously separated from background ions and molecular states of other species. The problem, then, becomes one of eliminating all possible sources of natural helium contamination from the sample gas and operating a very weak ion beam for extended periods.

Early work consistently underscored the problem of helium backgrounds. For example, a measurement carried out with a pure hydrogen plasma yielded a measurable mass-4 current and an easily detectable $^3He^{2+}$ count rate. The measured abundance was $\sim 10^{-8}$, consistent with natural contamination sources. When this background was scaled appropriately to the isotopically pure measurements, a background abundance of $\sim 10^{-12}$ would be implied. In an effort to eliminate background helium we have now built a new RF source that operates at high pressure and with good stability. The walls of the source are constructed from low helium diffusivity GE-180 and Uranium glass which is directly joined the the metal walls. All other source seals are metal. A gas handling system was constructed using two motor-controlled precision leak valves to allow gas samples to be changed without disturbing the operation of the source. In particular, this allows switching from pure hydrogen (used as both a guide beam and a test of contamination) to helium samples. With the new setup, we demonstrated good $^3H^{1+}$ production and beam stability. In addition, we produced a series of reference samples using natural helium measured to 1%. Measurements of these samples show good agreement with expectations. Finally we measured a set of ultra-pure samples from both the apparatus as well as a small quantity of gas from the original purification. Data analysis is still underway, however both samples show contamination at the few $\times 10^{-12}$ level. For reference, a purity of 5×10^{-12} would lead to a shift in the measured lifetime of 90 s.

As a result of uncertainties associated with purity issues as well as the loss of a significant fraction of our helium during warm-up after the last data collection run, we in the process of constructing our own helium purifier based on the design of the McClintock system, with the important distinction that nearly all components in the system on the ultra-pure side are now metal. This apparatus is in the final testing stages. The helium produced using the new purifier will be included in our upcoming purity measurements at ATLAS.

In support of further suppressing the effects of helium contamination, we also modeled, using a three-dimensional Navier-Stokes formalism, the transport of ^{3}He in ^{4}He at 400 mK via the heat flush technique. At this temperature, our dilution refrigerator has a cooling power of $\sim$ 6 mW. We have shown theoretically that by using an easily implemented smaller diameter tube to connect the measurement cell to the mixing chamber, one can reduce the ^{3}He concentration in the measurement cells by more than two orders of magnitude. (With our present geometry, we can reduce the concentration in the cell by a factor of ten). In addition, at these low temperatures, the vapor pressure of ^{3}He is considerably larger than that of ^{4}He, allowing us to preferentially pump away any remaining ^{3}He that is moved to the mixing chamber region.

With multiple approaches available and the proven purification technique,[15] we are confident that contamination of ^{3}He will ultimately not be a limiting factor in our lifetime measurement.

3.3. *Backgrounds*

Our detection system is sensitive to any mechanism that produces light. Thus, scintillation in the helium due to energetic charged particles as well as Compton scattering in the acrylic lightguides are potential backgrounds. These events arise from ambient radiation as well as both neutron-induced activation and luminescence. The ambient radiation gives rise to an overall constant background rate, while neutron-induced backgrounds are time dependent; some with timescales similar to the neutron lifetime. We now discuss our approach to reducing these backgrounds. All data presented here are preliminary. All figures show 20 pairs of trapping and non-trapping runs which corresponds to approximately four days of data collection.

Events are digitized and a timestamp is recorded for each. Corrections are made to the data for deadtime arising during readout of the digitizing cards and due to the hardware event veto. Corrections are applied to the pulse area and pulse height in response to the gain monitoring system. Several cuts are applied to remove background events. Initially, our electronics

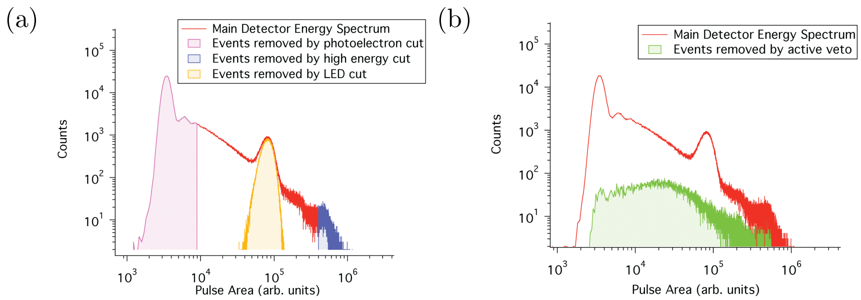

Fig. 4. (a) Application of threshold and pulser event cuts. (b) Removal of cosmic ray events.

require a coincidence between events in both photomultiplier tubes of the primary detector, thus all digitized data have events in both primary detector channels that pass a low-level voltage discrimination threshold. Events that are coincident with a separate detector that is part of the gain stabilization light pulser system are removed as can be seen in Fig. 4 (labeled as LED cut). This detector resides approximately 2 m from the apparatus and is shielded from any changes in magnetic fields generated by the apparatus. Cosmic ray events detected in external scintillators are then used to veto coincident events in the primary detector channels. (The placement of these scintillators can be seen in Fig. 1.) Fig. 4(b) shows the spectrum of events removed in this process. More restrictive upper and lower level software cuts are then applied to the pulse area to remove uncorrelated events related to neutron induced luminescence and pulse-shape distortion due to limited digitizer dynamic range respectively. These cuts are shown in Fig. 4(a). The lower level threshold was set to the equivalent of a 12 photoelectron between the two photomultiplier tubes. Work is still in progress to determine the optimum value for the upper-level threshold; we have used conservative cuts in the following discussion.

The resulting data are then analyzed in terms of pulse shape. The kurtosis - a gaussian parameter related to the fourth moment of the pulse shape - is used to separate different classes of events. One can observe in Fig. 5(a) two distinct peaks in the data. These correspond to events that occur in either the helium itself (lower value of kurtosis) or in the acrylic light guides (higher value of kurtosis). A threshold cut is made as indicated in the figure to remove events originating in the light guides. One can clearly see this separation of events when the same data is plotted as pulse area vs. pulse height; see Fig. 5(b). Events in blue are ones unaffected by the pulse

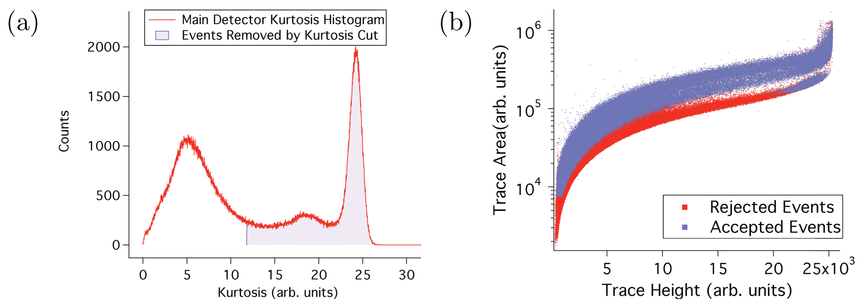

Fig. 5. (a) Events histogramed by gaussian kurtosis and illustrating pulse shape analysis of the data. (b) Two-dimensional plot of pulse area vs height; events in the lower band (associated with the plastic) not removed by the pulse shape cut are removed later with specific pulse height cuts.

shape cut, whereas red events correspond to events removed (i.e. having originated in the acrylic lightguides).

The resulting data after all corrections and all cuts have been applied is shown in Fig. 6. We expect that the mean number of photoelectrons for a neutron decay signal to be approximately 40 photoelectrons. In these data, the ambient radiation gives rise to an overall constant background event rate of order 70 s^{-1}. The neutron activation backgrounds yield time-dependent initial rates of order 10 s^{-1}. Since these are comparable in scale to the observed initial neutron decay count rate, 10 s^{-1}, an additional background subtraction procedure is required.

To accomplish this, two kinds of runs are performed; neutron trapping runs in which the magnetic field remains energized during both the trapping and observation periods, and background only runs where the field is energized only during the observation period and no neutrons are trapped during the loading phase. Data for each type of run is shown in Fig. 7.

One extracts the neutron lifetime by taking the difference between the data from the trapping and non-trapping runs. The result of this subtraction is shown in Fig. 7. In principle, one then directly fits this data to an exponential decay to extract the neutron lifetime.

Systematic effects related to imperfect background subtraction were previously investigated with data taken in the smaller apparatus when the isotopically-pure helium in the experimental cell was replaced with natural isotopic abundance helium. The resulting concentration of ^{3}He ($\approx 10^{-7}$) has a minimal effect on the neutron beam, and thus backgrounds, but the UCN trap-lifetime is shortened to less than 1 s as UCN are efficiently captured.

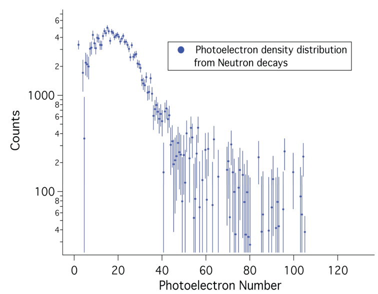

Fig. 6. Neutron trapping data after all background cuts from above (single channel).

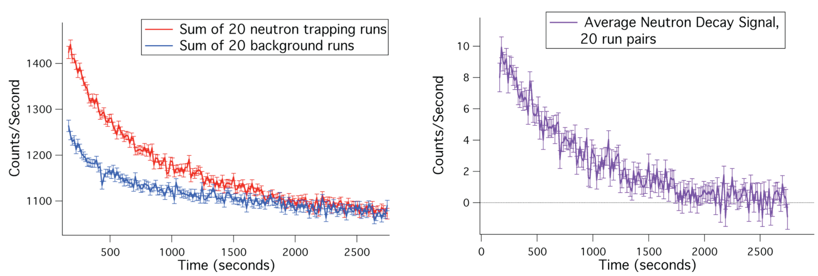

Fig. 7. Neutron trapping and non-trapping data after all background cuts (left) and the neutron decay signal after subtraction of trapping and non-trapping data runs (right).

The data taken were consistent with zero, thus providing confidence that the decay signals observed from the low-temperature runs with isotopically pure helium originate not from imperfect background subtraction, but from trapped neutrons. Similarly, one can raise the temperature in the trap to a point where thermal up-scattering reduces the trap lifetime to well below a second. Analysis of these data is underway, but preliminary results also support the efficacy of the background subtraction technique.

4. Conclusions

The neutron decay curves extracted from 300 mK data collected using our new apparatus exhibit a trap lifetime that has a significant shift due to some, as yet, unexplained systematic effect that suggests that there exist neutron trap loss mechanisms other than beta decay. Runs where the magnetic fields are ramped to remove marginally trapped neutrons have not been able to explain this discrepancy. However as discussed above, based on recent results from the AMS measurements on the ultra-pure helium produced by McClintock, we believe that losses due to the presence of small amounts of ^{3}He in our isotopically purified ^{4}He is a likely candidate.

A significant benefit of the new apparatus is that the increased countrates give us time to perform systematic checks such as measuring the neutron loss due to phonon up-scattering, the elimination of above threshold neutrons, and a careful characterization of imperfect background subtraction. Going forward, we intend to purify a new sample of ultrapure helium, and, using this sample continue with our systematic studies of marginally trapped neutrons.

Assuming our apparatus operates as it has previously, and taking advantage of several opportunities for improvement, we anticipate that we will be able to perform a 0.5 % lifetime measurement in 18 days, or equivalently, a measurement with a statistical uncertainty corresponding to < 3 s in a 40 day reactor cycle. Such a measurement would yet play an important role in clarifying the current uncertainty surrounding the neutron lifetime as the systematic uncertainties are very different than those of other experiments.

References

1. J. M. Doyle and S. K. Lamoreaux, *Europhysics Letters* **26**, 253 (1994).
2. R. Golub and J. M. Pendlebury, *Physics Letters* **53A**, 133 (1975).
3. D. N. McKinsey, et al., *Physical Review A* **67**, 062716 (2003).
4. D. N. McKinsey, et al., *Physical Review A* **59**, 200 (1999).
5. S. Arzumanov *et al.*, *Phys. Lett. B* **483**, 15 (2000).
6. J. S. Adams et al., *J. of Low Temp. Phys*, **13**:1121, (1998)
7. Certain trade names and company products are mentioned in the text or identified in illustrations in order to adequately specify the experimental procedure and equipment used. In no case does such identification imply recommendation or endorsement by the National Institute of Standards and Technology, nor does it imply that the products are necessarily the best available for the purpose.
8. J. M. Lock, *Cryogenics* **9** 438, (1969).
9. J. S. Butterworth *et al.*, *Rev. Sci. Instrum.* **69**, 3998 (1998).
10. L. Yang, PhD thesis, Harvard University, 2006.
11. C. M. Oshaughnessy, PhD thesis, North Carolina State University, 2010.
12. K. J. Coakley *et al.*, *J. Res. Natl. Inst. Stand. Techol.* **110** 367, (2005).
13. *Ultra-Cold Neutrons*, R. Golub, D. Richardson and S. K. Lamoreaux, OP Publishing Ltd., (1991)
14. F. Pobell. *Matter and Methods at Low Temperatures.* 2nd edition. Springer-Verlag, Berlin, 1996.
15. P. V. E. McClintock, *Cryogenics* **18** 201, (1978).